Copper nanoparticle formation in a reducing gas environment

ten Brink, Gert H.; Krishnan, Gopi; Kooi, Bart J.; Palasantzas, George

Published in:
Journal of Applied Physics

DOI:
10.1063/1.4895483

Publication date:
2014

Copper nanoparticle formation in a reducing gas environment

Gert H. ten Brink, Gopi Krishnan, Bart J. Kooi, and George Palasantzas

Citation: Journal of Applied Physics **116**, 104302 (2014); doi: 10.1063/1.4895483
View online: https://doi.org/10.1063/1.4895483
View Table of Contents: http://aip.scitation.org/toc/jap/116/10
Published by the American Institute of Physics

JOURNAL OF APPLIED PHYSICS **116**, 104302 (2014)

Copper nanoparticle formation in a reducing gas environment

Gert H. ten Brink,[a] Gopi Krishnan, Bart J. Kooi, and George Palasantzas
Zernike Institute for Advanced Materials and the Materials innovation institute (M2i), University of Groningen, Nijenborgh 4, 9747 AG Groningen, The Netherlands

(Received 8 July 2014; accepted 31 August 2014; published online 9 September 2014)

Although copper nanoparticles are used as model nanomaterial because of their small nucleation barrier, their oxidization sensitivity hampers production of fully *metallic* nanoparticles with controlled size and shape. Nevertheless, we demonstrate here synthesis of copper nanoparticles, via high pressure magnetron sputtering, having highly tunable sizes and shapes over a size range spanning two orders of magnitude. This is achieved by exploiting a reducing gas environment to mediate proper nucleation conditions, allowing size control of nanoparticles with robust motifs for particle sizes ~5–300 nm. However, due to rapid coalescence oxidation-free nanoparticles cannot be produced monodisperse for sizes larger than ~30 nm. © *2014 AIP Publishing LLC*.
[http://dx.doi.org/10.1063/1.4895483]

I. INTRODUCTION

Nowadays, nanoparticles (NPs) have emerged as key materials for important modern day applications in plasmonics, catalysis, biodiagnostics, and nanomagnetics.[1–7] To produce NPs, a number of techniques are available either as a top down or a bottom up approach. Among all techniques magnetron sputtering has emerged as a mature and good candidate for clean NPs science.[6,8–11] Nevertheless, even under clear vacuum conditions, a wide variety of studies have shown that impurities play an important role in the nucleation and subsequent growth of NPs, as well as in the structural motifs they may develop. In fact, for copper (Cu) NPs an early *in situ* transmission electron microscope (TEM) study has shed light on the effects of oxygen in the early stages of sintering, coalescence, and morphology. It was shown that NPs produced under clean conditions experience substantial sintering and grain growth upon contact, even at room temperature, while NPs exposed to traces amounts of oxygen remained distinct.[12–16] Therefore, if rapid sintering occurs, it can be difficult to form ultraclean metal nanophase materials.[12–16]

Further studies for Cu NPs indicated that the NPs grow upon oxygen exposure, which slows sintering and alters the structure of the NPs, by Brownian coagulation to produce self-similar distributions.[14–16] This model confirmed the role of oxygen inhibiting surface diffusion processes, and the NP size distribution approached the common log-normal distribution.[17–20] It was concluded that oxygen impurities may be desirable to limit agglomeration and to permit dense NP compact formations. Furthermore, an interaction has been observed between Cu NPs and amorphous carbon which produces graphite shells.[12] The shell formation suggested a solid state analog to that when NPs catalyze the growth of carbon fibers via decomposition in a hydrocarbon atmosphere.[12] Oxidation studies of Cu NPs with sizes less than 10 nm by TEM have revealed that beginning with multiple twinned particles as stable structures for NPs with diameters less than 5 nm, and of cube-octahedral for larger NPs, then in the transitional state between pure metal and oxide both states can coexist within the same particle.[15,16,21] The creation of sub-oxides with lower reactivity than the pure metal NPs could also lead to morphologies, which are different from the pure metal.[15,16,21,22]

However, it still remains obscure how the transition between an oxidizing environment to a carbon or hydrogen based reducing atmosphere can influence the nucleation and growth of oxidation sensitive metal NPs. Indeed, Cu NPs have not only been a subject of various oxidizing studies in the past but also they have a small nucleation barrier making them suitable as a model nanomaterial.[23] Without any preventive measure, Cu NPs formed during high pressure magnetron sputtering within a vacuum system (with base pressure $\sim 10^{-9}$ mbar that is close to ultra-high vacuum) are highly oxidized because the experimental setup still contains enough oxygen and water.[24] In fact, it is known that carbon deposition on the Cu target surface can prevent surface oxidization.[25] The presence of carbon also plays a role in the NP formation process.[26,27] This is because C atoms can be adsorbed on the primary NP nucleus aiding the coalescence processes during high pressure magnetron sputtering of Cu, and in the final stages can diffuse out of the NPs forming a thin carbon layer, which helps to prevent rapid oxidization under atmospheric conditions.[26–28] As it will be shown in the following, a carbon or hydrogen based reducing gas environment can remove the strong effect of oxygen and enhance both the size control of NPs and quality of structural motifs in the size range of 5–300 nm (see supplementary material for the NP size distributions[29]). This size range is unique for this type of high pressure magnetron sputtering and to our knowledge has not been shown before due to the fact that oxidation is normally limiting the final NP-sizes.

II. EXPERIMENTAL METHODS

The initial Cu NPs produced with a high pressure magnetron sputtering source (see supplementary material for the NP deposition system in Fig. 2S[29]) had limited sizes in the range of about 1–30 nm. The size of NPs could be altered,

[a]Author to whom correspondence should be addressed. Electronic mail: g.h.ten.brink@rug.nl

e.g., by changing the aggregation length, the pressure and type of gas (argon and helium), and magnetron power.[23,30–32] The NPs were deposited on either (holey) carbon coated Cu grids or on a 20 nm thick silicon nitride membranes. Careful TEM/EDX[33] (Energy Dispersive X-ray, see supplementary material for the EDAX analysis[29]) analysis was performed to address the oxidation state and structure of the NPs. In fact, the NPs were characterized with a JEOL 2010F TEM and/or an FEI Tecnai C^2 both operating at 200 kV. The obtained TEM images were statistically processed by Image-Pro Plus v.7 software[34] to obtain the NP size distributions (see supplementary material for the NP size distributions[29]). The latter were also fitted by the log-normal size distribution using MATLAB routines[35,36]

$$f_X(x;\mu,\sigma) = \frac{1}{x\sigma\sqrt{2\pi}} e^{-\frac{(\ln x-\mu)^2}{2\sigma^2}} \quad (x > 0), \tag{1}$$

in order to verify that the typical NP growth process takes place during high pressure magnetron sputtering by condensation of a supersaturated vapor, where the growth rate is independent of size. In Eq. (1), the parameters μ and σ are, respectively, the mean and standard deviation of ln(x) with x the particle size. The actual standard deviation of the particle sizes $\Delta\sigma$ as a function of μ and σ is given by $\Delta\sigma = \sqrt{\exp(\sigma^2) - 1}\,\exp(\mu + \sigma^2/2)$.[36]

III. RESULTS AND DISCUSSION

Figure 1 shows a bright field TEM image of as-deposited Cu NPs without introduction of any other gas except Ar for sputtering into the deposition system. The size of the NPs was limited to ~10–30 nm (see also Fig. 6S in supplementary material[29]), which appeared to be a common outcome for any achievable operating window of the deposition source. The first impression in Figure 1 is that the NPs appear to have normal shape and structure. However, closer inspection reveals that they are nearly spherical agglomerates, and they are largely oxidized with only smaller crystalline inner cores in the primary NPs forming the agglomerate. This is also confirmed with EDX analysis (see Figure 3S in supplementary material for the EDAX analysis[29]), where, however, some variation has been documented for different depositions. Although Cu (together with Ag and Au) is in group 11 of the periodic table, the high reactivity of NPs makes them sensitive to oxidization.[27,28] In addition, also NPs with cubic (square in projection) crystal habit were observed (see Fig. 6S in supplementary material[29]), which is indicative that the Cu is oxidized. The NPs are basically truncated octahedral structures and become cubic, square in projection, only when they are formed in the presence of oxygen. Indeed, oxygen exposure deepens the (100) and (111) cusps of the γ-plot (Wulff construction) for Cu.[13,37,38] Without oxygen interference, Cu NPs would grow into icosahedral multiple twinned particles since it is energetically the most favorable state for fcc Cu with NP sizes ~5–30 nm.[39]

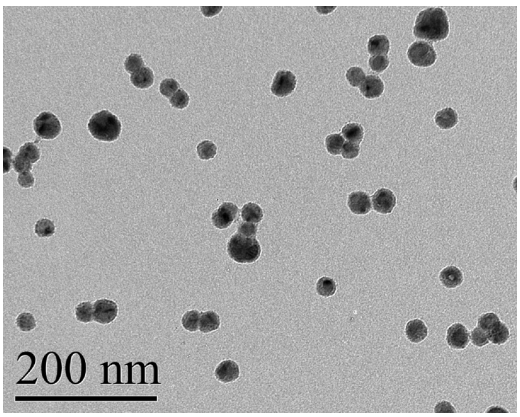

FIG. 1. Bright field TEM image of as-deposited Cu NPs without deliberate any other gas than Ar 5.0 present during the deposition. The image seems to indicate successful NP formation, but closer inspection reveals largely oxidized NPs forming agglomerates.

Recent research has suggested that oxygen plays a crucial role for NP nucleation but it hinders NP growth.[14,32] Although in our former studies using a similar deposition system (an Oxford NC200B deposition source at a base pressure ~5×10^{-8} mbar) we have produced Cu crystalline NPs with an ultrathin (~1–2 nm thick) outer oxide shell,[40–42] the oxidation situation in the present system remained unaltered even by excellent bake-out and introduction of higher grade sputtering gas. In practice, only a few options remained to eliminate sources of water or oxygen inside a vacuum system and limit the oxidation of NPs.[24] However, small amounts of impurities aid NP formation.[32] Therefore, when we tried to remove all possible sources of oxygen and water contaminations within the deposition system, the nucleation of NPs was completely blocked under normal operating conditions (e.g., as in Fig. 1).

To overcome this nucleation problem and form crystalline Cu NPs with controlled size, a reducing gas, e.g., methane or hydrogen, was used to remove or minimize any remnant oxidizing impurities from the system (but still allowed or aided NP nucleation). A small amount of methane or hydrogen into the magnetron plasma during sputtering would react *in situ* with remnant water and oxygen and convert it into volatile species which could be pumped away.[43] Therefore, after system bake out to achieve ~5×10^{-9} mbar base pressure, a small amount of methane or hydrogen gas was introduced, by means of a high precision UHV-leak valve, in the aggregation chamber up to a pressure of ~2×10^{-5} mbar or less. Direct measurement of the methane or hydrogen partial pressure during sputtering was not possible because the magnetron is operated at a higher Ar pressure for sputtering (~0.5 mbar). The NP production took place within the normal operating window (e.g., 20–40 sccm argon which equals 0.30–0.50 mbar; depending also on the size of the aperture used, see Fig. 2S in supplementary material for the NP deposition system[29]).

The direct partial oxidation of methane to synthesis gas proceeds exothermic and endothermic via the reactions[43]

$$\begin{aligned} CH_4 + \frac{1}{2}O_2 &\rightarrow CO + 2H_2 \,(\Delta H = -22.1\,\mathrm{kJ/mol}), \\ CH_4 + H_2O &\leftrightarrow CO + 3H_2 \,(\Delta H = 226\,\mathrm{kJ/mol}). \end{aligned} \tag{2}$$

The high temperatures (~1000 K) needed for the endothermic conversion are easily achieved inside the magnetron plasma during sputtering[44–46]

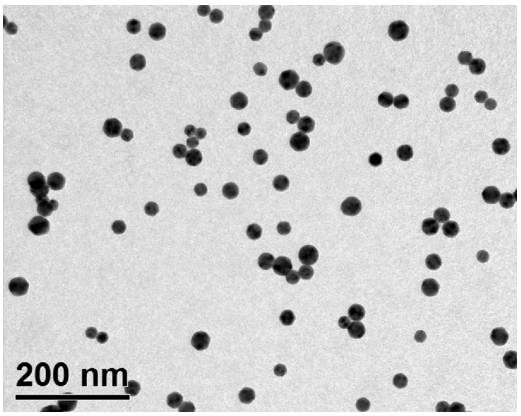

FIG. 2. Bright field TEM image of as-deposited Cu NPs with 2×10^{-5} mbar methane and Ar 6.0 present during the deposition. Metallic NPs are formed with a proper multiple twinned near-icosahedral structure.

$$H_2 + \frac{1}{2}O_2 \rightarrow H_2O\,(\Delta H = -248\,\mathrm{kJ/mol}),$$
$$CO + \frac{1}{2}O_2 \rightarrow CO_2\,(\Delta H = -283\,\mathrm{kJ/mol}). \qquad (3)$$

Subsequent reactions with CO and H_2 will form CO_2 and H_2O which can be pumped away. The byproduct of gas synthesis, i.e., carbon, aids the system in multiple ways. Carbon deposition as byproduct can in return prevent the sputtering target from corrosion ($CH_4 \leftrightarrow C + 2\ H_2$ ($\Delta H = -89.9$ kJ/mol)).[25] Carbon also plays a role in the formation process of NPs.[27] Indeed, C atoms can be adsorbed on the primary NP nucleus aiding in the coalescence process, and in the final stage diffuse out of the NP forming a thin carbon layer which prevents quick oxidization under atmospheric conditions.[23,47] In a similar way, hydrogen used as a reducing gas can also react with remnant oxygen.

The resulting NPs (Figs. 2–5) clearly show the effect of the reducing gas environment. Oxide containing aggregates are not formed and NPs now have a multiple twinned near-icosahedral structure as should be the case for clean NPs (not influenced by oxidation). Moreover, EDX analysis showed an apparent absence of oxygen (see Figs. 4S and 5S in supplementary material for the EDAX analysis[29]). In the case of Cu NPs made with a small amount of hydrogen gas, no oxide shell could be detected (see Fig. 5). Cu NPs made with a small amount of methane gas were generally still surrounded by an ultra-thin ~2 nm thick Cu_2O shell. High resolution TEM (HRTEM) analysis revealed also the presence of an ultra-thin (~2 nm) layer of carbon. This finding can be understood, because, according to the C-Cu phase diagram, C cannot be dissolved within bulk Cu ($\ll$0.001 at. %)[48] and when present during nucleation is pushed outside during growth, where of course the situation might be different for NPs compared to bulk. Still, the use of methane reducing gas environment for production of metallic NPs, in general, is

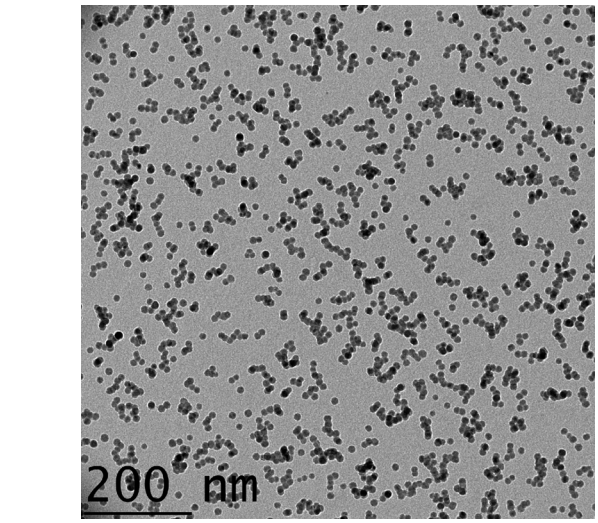

FIG. 4. Bright field TEM image of as-deposited Cu NPs with 2×10^{-5} mbar hydrogen and Ar 6.0 present during the deposition. Monodisperse metallic Cu NPs are formed with log-normal distribution peaked at 12 nm, and with standard deviation below 3 nm.

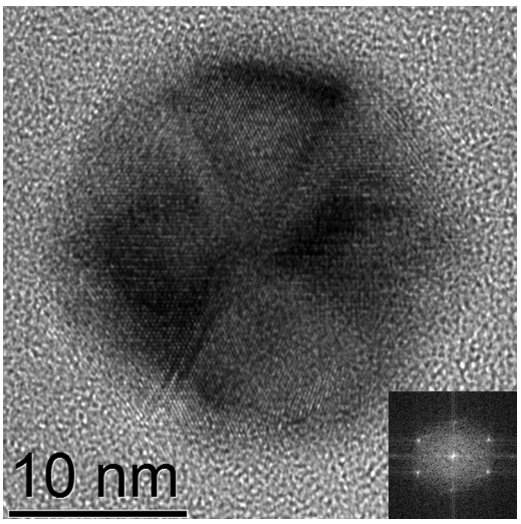

FIG. 3. HRTEM image from one Cu NP in Fig. 2 showing an icosahedron shaped multiple twinned particle, the insert FFT of part of the particle is showing lattice spacings d = 0.18 and d = 0.21 nm, which are the d_{200} and d_{111} of metallic Cu, respectively.

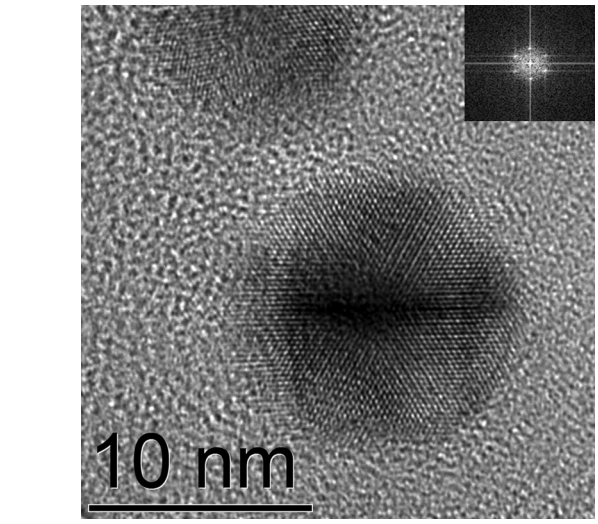

FIG. 5. HRTEM image from one Cu NP in Fig. 4 showing an icosahedron shaped multiple twinned particle, the insert FFT of part of the particle is showing lattice spacings d = 0.21 nm, which is the d_{111} of icosahedron, three-fold axis metallic Cu.

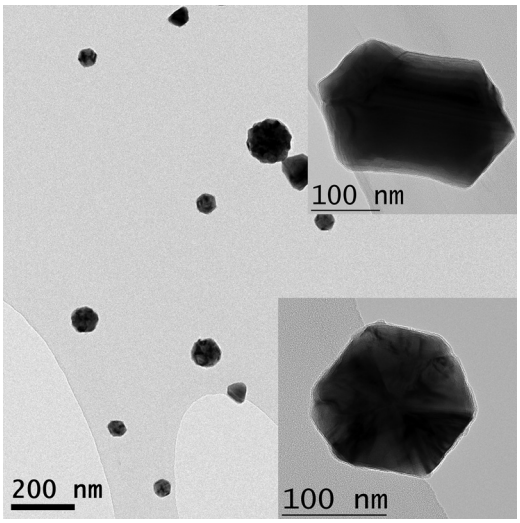

FIG. 6. Bright field TEM image of as-deposited Cu NPs with high purity Ar 6.0 for sputtering and 2×10^{-5} mbar CH_4 during the deposition using the longest aggregation length (13 cm). Cu NPs with sizes of over 300 nm are formed.

expected to be limited to metals showing a low carbon solubility and of course metals which are not too strong carbide formers although we have obtained good results with it for iron NPs as well.

Moreover, important generalized findings for the reducing environment are the following. A short aggregation length (5 cm) in the dedicated nanoparticle source leads to a particle size of ~10 nm with rather monodisperse size distribution. Smaller particles (<10 nm) can be made using helium (in addition to argon) to increase NP cooling. The maximum aggregation length (13 cm) gives a NP-size range up to ~300 nm (see Fig. 6) with the remark that for the longer aggregation length the size distribution is not monodisperse anymore. This can be expected, because the icosahedron-based pure Cu NPs can rapidly coalesce, because not interfered by oxygen shells of the primary NPs. Only by introducing excess methane the size limiting role of oxygen is taken over by carbon at the surface of the primary NPs preventing their rapid coalescence.

In any case, Fig. 7 shows an overview of the different stages that can be identified during the NP formation.[49] First, nucleation takes place on a critical cluster size $r^* = 2\sigma_e m/kT\rho\ln(\varphi)$.[49,50] σ_e stands for the surface energy of a small droplet of atoms, ρ is its density, m is its atomic or molecular mass, and $\varphi = p_k/p_s$ is its condition for super saturation (p_k and p_s are the vapor and saturation vapor pressure, respectively). For larger radii, accretion of atoms on the small cluster becomes thermodynamically favorable leading to rapid growth. Depending on the amount of remnant oxygen and water in the system, NPs agglomerates are formed from primary particles, e.g., small particles, in which the primary particles remain identifiable being Cu NPs with a thin oxide shell (see Fig. 7(a) and HRTEM inset and also Fig. 1). Then, Figs. 7(b)–7(d) show results of a gradual increasing methane addition to the aggregation chamber. Due to less surface oxidization, accretion[50] and coalescence takes place and bigger particles are formed. However, there is still a thin oxide layer preventing further coalescence (Fig. 7(b)).

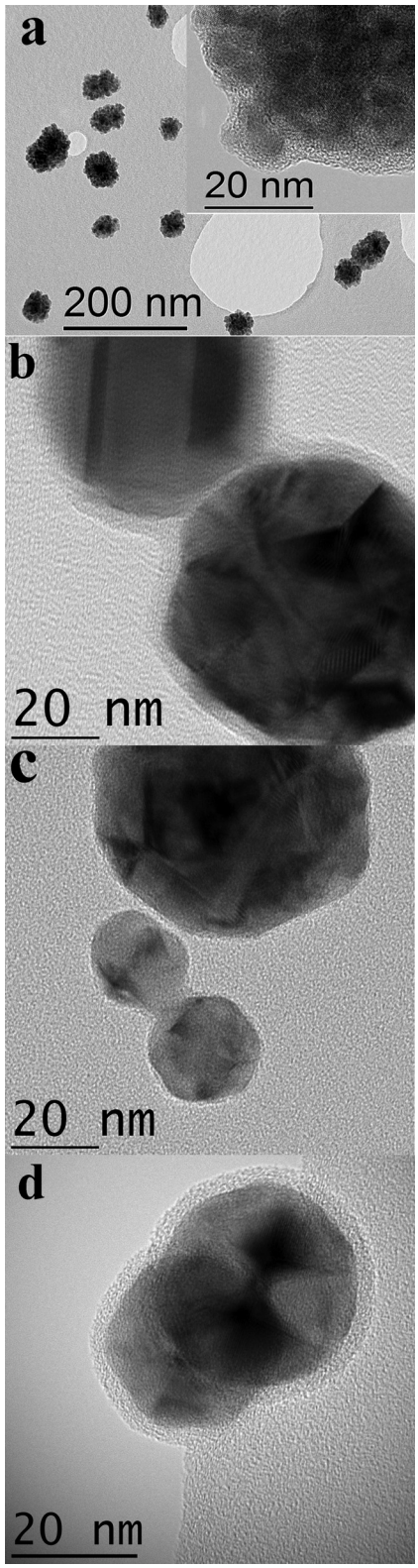

FIG. 7. Bright field TEM overview of the different stages in the coalescence and agglomeration process of deposited Cu NPs with increasing amounts of methane (from a → d)) during deposition. (a) NPs agglomerates are formed from primary Cu NPs with thin oxide shells as it is shown in the inset. (b) Higher methane content in the aggregation chamber: accretion and coalescence to form bigger particles. Remnant amounts of oxygen are still present and produce a thin oxide layer thereby hindering further coalescence. (c) An intermediate condition with a thinner oxide layer than in (b). Coalescence is taking place, while the necking is clearly visible without grain boundary formation. (d) Higher methane addition is leading to NP formation with excess of carbon, which limits effectively the NP size to grow further.

Figure 7(c) shows an even thinner oxide layer than that in Fig. 7(b), where coalescence is taking place. Here, the necking is clearly visible but no grain boundary is yet formed. Under normal operating conditions (e.g., ~0.3–0.5 mbar sputtering gas depending also on the exit aperture of the aggregation volume, see supplementary material for the NP deposition system[29]), distinct facetted NPs are formed with good size control as can be seen from the overview in Fig. 2 (and Fig. 7(d) for more details of the NPs structure). In Fig. 7(d), it becomes apparent that with excess methane a clear carbon-based shell is formed around metallic multiple twinned (near icosahedral) Cu particles.

IV. CONCLUSIONS

Cu nanoparticles can be synthesized with high pressure magnetron sputtering having tunable sizes and shapes as high-resolution transmission electron microscopy demonstrated. Although Cu NPs are used as a model material because of their small nucleation barrier, their oxidization sensitivity makes it difficult to control sizes of purely metallic NPs over large ranges. However, with the aid of a reducing gas environment to minimize NP oxidization (by removing oxygen and water), we can achieve a proper NP nucleation conditions to form metallic NPs. Moreover, we can enhance the size control of these NPs leading to relatively narrow size distributions and robust (near icosahedral) structural motifs for particle sizes up to ~30 nm. Metallic NPs with sizes as large as 300 nm can be readily produced because coalescence of primary NPs in the reducing atmosphere is not prevented by the presence of oxide shells. However, in the case of excess methane the high carbon content limits the NPs to grow further in size.

ACKNOWLEDGMENTS

We would like to acknowledge support by the Materials innovation institute M2i and the Zernike Institute for Advanced Materials.

[1]P. D. U. Kreibig and P. D. M. Vollmer, *Optical Properties of Metal Clusters* (Springer, Berlin, 1995).
[2]E. Prodan and P. Nordlander, Nano Lett. **3**, 543 (2003).
[3]J. P. Wilcoxon and B. L. Abrams, Chem. Soc. Rev. **35**, 1162 (2006).
[4]*Nanomaterials: Synthesis, Properties and Applications*, 2nd ed., edited by A. S. Edelstein and R. C. Cammaratra (Taylor & Francis, 1998).
[5]C. Binns, Surf. Sci. Rep. **44**, 1 (2001).
[6]P. Jensen, "Growth of nanostructures by cluster deposition: A review," Rev. Mod. Phys. **71**(5), 1695 (1999).
[7]W. A. de Heer, Rev. Mod. Phys. **65**, 611 (1993).
[8]C. Xirouchaki and R. E. Palmer, Philos. Trans. R. Soc., A **362**, 117 (2004).
[9]P. J. Kelly and R. D. Arnell, Vacuum **56**, 159 (2000).
[10]K. Wegner, P. Piseri, H. V. Tafreshi, and P. Milani, J. Phys. D: Appl. Phys. **39**, R439 (2006).
[11]P. Jensen and N. Combe, Comput. Mater. Sci. **24**, 78 (2002).
[12]D. L. Olynick, J. M. Gibson, and R. S. Averback, Mater. Sci. Eng., A **204**, 54 (1995).
[13]D. L. Olynick, J. M. Gibson, and R. S. Averback, Appl. Phys. Lett. **68**, 343 (1996).
[14]D. L. Olynick, J. M. Gibson, and R. S. Averback, Philos. Mag. A **77**, 1205 (1998).
[15]J. Urban, H. Sack-Kongehl, and K. Weiss, Z. Phys. D: At., Mol. Clusters **36**, 73 (1996).
[16]J. Urban, H. Sack-Kongehl, and K. Weiss, Catal. Lett. **49**, 101 (1997).
[17]L. B. Kiss, J. Söderlund, G. A. Niklasson, and C. G. Granqvist, Nanotechnology **10**, 25 (1999).
[18]L. B. Kiss, J. Söderlund, G. A. Niklasson, and C. G. Granqvist, Nanostruct. Mater. **12**, 327 (1999).
[19]C. G. Granqvist and R. A. Buhrman, Solid State Commun. **18**, 123 (1976).
[20]C. G. Granqvist and R. A. Buhrman, J. Appl. Phys. **47**, 2200 (1976).
[21]I. Lisiecki, A. Filankembo, H. Sack-Kongehl, K. Weiss, M.-P. Pileni, and J. Urban, Phys. Rev. B **61**, 4968 (2000).
[22]S. Giorgio and J. Urban, *Small Particles Inorganic Clusters* (Springer, 1989), pp. 115–118.
[23]M. Gracia-Pinilla, E. Martínez, G. S. Vidaurri, and E. Pérez-Tijerina, Nanoscale Res. Lett. **5**, 180 (2009).
[24]V. A. Vons and A. Schmidt-Ott, "Spark Discharge Generated Nanoparticles for Hydrogen Storage Applications," (Delft University of Technology, 2010).
[25]A. Majumdar, J. F. Behnke, R. Hippler, K. Matyash, and R. Schneider, J. Phys. Chem. A **109**, 9371 (2005).
[26]C. Hao, F. Xiao, and Z. Cui, J. Nanopart. Res. **10**, 47 (2008).
[27]S. Wang, X. Huang, Y. He, H. Huang, Y. Wu, L. Hou, X. Liu, T. Yang, J. Zou, and B. Huang, Carbon **50**, 2119 (2012).
[28]G. Cheng and A. R. Hight Walker, Anal. Bioanal. Chem. **396**, 1057 (2010).
[29]See supplementary material at http://dx.doi.org/10.1063/1.4895483 for NP deposition system, EDAX analysis, and NP size distributions.
[30]A. N. Banerjee, R. Krishna, and B. Das, Appl. Phys. A **90**, 299 (2007).
[31]A. Majumdar, D. Köpp, M. Ganeva, D. Datta, S. Bhattacharyya, and R. Hippler, Rev. Sci. Instrum. **80**, 095103 (2009).
[32]A. Marek, J. Valter, S. Kadlec, and J. Vyskočil, Surf. Coat. Technol. **205**(Suppl. 2), S573 (2011).
[33]G. L. Hornyak, S. Peschel, T. Sawitowski, and G. Schmid, Micron **29**, 183 (1998).
[34]See http://www.mediacy.com/ for Computer Program Image-Pro Plus.
[35]See http://www.mathworks.nl/products/matlab/ for Computer Program MATLAB.
[36]S. Kotz, N. Balakrishnan, and N. L. Johnson, *Continuous Univariate Distributions*, 2nd ed. (Wiley, New York, 1994); C. Binns, *Introduction to Nanoscience and Nanotechnology* (Wiley, New York, 2010).
[37]B. E. Sundquist, Acta Metall. **12**, 67 (1964).
[38]B. E. Sundquist, Acta Metall. **12**, 585 (1964).
[39]S. Ino, J. Phys. Soc. Jpn. **27**, 941 (1969).
[40]G. Krishnan, G. Palasantzas, and B. J. Kooi, Appl. Phys. Lett. **97**, 131911 (2010).
[41]G. Palasantzas, S. A. Koch, and J. T. De Hosson, Rev. Adv. Mater. Sci. **5**, 57 (2003).
[42]G. Palasantzas, S. A. Koch, and J. T. M. De Hosson, Appl. Phys. Lett. **81**, 1089 (2002).
[43]C. R. H. de Smet, "Partial oxidation of methane to synthesis gas: reaction kinetics and reactor modelling," (Technische Universiteit Eindhoven, 2000).
[44]E. Quesnel, E. Pauliac-Vaujour, and V. Muffato, J. Appl. Phys. **107**, 054309 (2010).
[45]E. Pauliac-Vaujour, E. Quesnel, and V. Muffato, in *Materials Challenges in Alternative and Renewable Energy*, edited by G. Wicks, J. Simon, R. Zidan, E. Lara-Curzio, T. Adams, J. Zayas, A. Karkamkar, R. Sindelar, and B. Garcia-Diaz (John Wiley & Sons, Inc., 2010), pp. 163–172.
[46]B. Chapman, *Glow Discharge Process* (Wiley, 1980).
[47]C.-H. Chen, T. Yamaguchi, K. Sugawara, and K. Koga, J. Phys. Chem. B **109**, 20669 (2005).
[48]G. A. López and E. J. Mittemeijer, Scr. Mater. **51**, 1 (2004).
[49]R. C. Flagan and M. M. Lunden, Mater. Sci. Eng., A **204**, 113 (1995).
[50]P. Feiden, J. Leygnier, P. Cahuzac, and C. Bréchignac, Eur. Phys. J. D **43**, 49 (2007).